# Stellar Models including pre-SN/SN phases

Alexander Heger [a], S. E. Woosley [a], Norbert Langer [b],

[a] *Astronomy Department, University of California, Santa Cruz, CA 95064, U. S. A.*

[b] *Institut für Theoretische Physik und Astrophysik, Universität Potsdam, Am Neuen Palais 10, 14469 Potsdam, Germany*

**Abstract**

We present a grid of new models of rotating and non-rotating stars of solar metallicity. Their evolution was followed form the pre-main sequence stage up to core collapse using a 199 isotope network. The evolution and nucleosynthesis was continued through the supernova stage using a "piston" model (18) to simulate the explosion. Final isotopic yields are given for 15 and $25\,\mathrm{M}_{\odot}$ stars with different assumptions regarding the mixing efficiency of semiconvection and for rotating and non-rotating stellar models.

*Key words:* stellar evolution; rotation; nucleosynthesis; supernovae

## 1 Introduction

Massive stars above $\sim 10\,\mathrm{M}_{\odot}$ are the main producers of oxygen and heavier elements. A study of massive stellar models of various masses and metallicities including their nucleosynthetic yields was performed earlier by (18). However, those models neglected mass loss from the stellar surface and rotation.

Mass loss, generally, tends to reduce the nucleosynthetic processing in a star by removing less processed mass from its surface and thereby leading to smaller cores with smaller (convectively) burning regions. One example is core hydrogen burning, where smaller initial helium cores are obtained as a result of the mass loss. Another important case is that of "early" type Wolf-Rayet stars, where the helium core itself is shrunk by the mass loss, which affects both the size and the initial carbon content of the helium-free core (CO core) resulting after the end of central helium burning.

Rotation, on the other hand, tends to induce additional mixing processes that increase the core masses. This is due to localized mixing at the edges of convective regions and large-scale circulation (see also the contribution by A. Maeder in this volume) which enhances the mean molecular weight in convectively stable regions that would not be mixed in non-rotating stars. In some burning environments, in particular those related to hydrogen burning, new nucleosynthesis channels can be opened by mixing chemical species that would not be mixed in non-rotating stars.

Besides rotation, the uncertain efficiency of semiconvection and the amount of overshooting also play a major role, as they determine the persistence of the boundaries of convective layers. In case of "slow" semiconvection a molecular weight barrier can form which splits the convective helium core and leads to smaller CO cores than result in the case of "fast" semiconvection (17; 14). Semiconvection also affects the helium gradients at the top of the CO core and the evolution of the convective helium shell.

The present paper is based upon a study of eight stellar models. We investigated 15 and 25 $M_\odot$ stars with an initial metallicity of 2 % and solar abundance ratios (5). For each mass we simulated rotating and non-rotating models, each of which employed two different assumptions for the efficiency of semiconvective mixing. A more detailed presentation of our results will be given in (8).

In the next section we give a brief overview over the input physics and numerical method used. In § 3 the results of the nucleosynthesis calculations will be presented. In the last section we give our conclusions and an outlook on future work.

## 2 Input physics and numerical method

The numerical simulations were performed using hydrodynamic stellar evolution code (15, KEPLER). Rotationally induced mixing processes and angular momentum redistribution was included as in (7). In addition to convection and semiconvection, both chemical mixing and angular momentum transport were included to account for Eddington-Sweet circulation, the Goldreich-Schubert-Fricke instability, secular and dynamical shear instabilities, and the Solberg-Høiland instability (1; 7). The uncertain efficiencies of mixing and angular momentum transport of these instabilities were gauged to reproduce typical observed surface enrichments of massive stars during central hydrogen burning for typical initial rotation rates (13; 7). All rotating models in the present work have a rotational velocity of $\sim 200\,\mathrm{km\,s^{-1}}$ an the zero-age main sequence (ZAMS), which is a typical value for these stars (4). A overview of the properties of all models is given in Table 1.

Table 1
Initial model properties (mass, semiconvection, overshooting, ZAMS rotation velocity) and final stellar mass and iron core mass. The last two columns give the location of the piston (in mass) used to simulate the supernova explosion, and the amount of fallback after the explosion. For comparison the two models S15A and S25A of (18) are given as well.

| Model (mass) | $M_{\mathrm{ZAMS}}$ ($\mathrm{M}_{\odot}$) | $\alpha_{\mathrm{sem}}$ | osht ($H_P$) | $v_{\mathrm{ZAMS}}$ ($\mathrm{km\,s^{-1}}$) | $M_{\mathrm{preSN}}$ ($\mathrm{M}_{\odot}$) | Fe core ($\mathrm{M}_{\odot}$) | piston ($\mathrm{M}_{\odot}$) | fallback ($\mathrm{M}_{\odot}$) |
|---|---|---|---|---|---|---|---|---|
| S15A | 15.082 | 0.1 | 0.01 | 0 | 15.082 | 1.32 | 1.32 | 0.00 |
| db15 | 15 | $10^{-4}$ | 0 | 0 | 13.542 | 1.33 | 1.33 | 0.006 |
| dc15 | 15 | 0.1 | 0.01 | 0 | 12.358 | 1.56 | 1.56 | 0.080 |
| eb15 | 15 | $10^{-4}$ | 0 | 200 | 13.155 | 1.32 | 1.29 | 0.045 |
| ec15 | 15 | 0.1 | 0.01 | 200 | 11.948 | 1.35 | 1.29 | 0.188 |
| S25A | 25.137 | 0.1 | 0.01 | 0 | 25.137 | 1.78 | 1.78 | 0.29 |
| db25 | 25 | $10^{-4}$ | 0 | 0 | 17.506 | 1.41 | 1.41 | 0.25 |
| dc25 | 25 | 0.1 | 0.01 | 0 | 13.215 | 1.67 | 1.67 | 0.056 |
| eb25 | 25 | $10^{-4}$ | 0 | 200 | 14.632 | 1.90 | 1.97 | 0.00 |
| ec25 | 25 | 0.1 | 0.01 | 200 | 10.562 | 1.81 | 1.84 | 0.00 |

Table 2
Updated reaction rates

| | | | | |
|---|---|---|---|---|
| $^{9}$Be($\alpha$,n)$^{12}$C | $^{18}$O($\alpha,\gamma$)$^{22}$Ne | $^{22}$Ne(p,$\gamma$)$^{23}$Na | $^{27}$Al(p,$\alpha$)$^{24}$Mg | $^{27}$Al(p,$\gamma$)$^{28}$Si |
| $^{13}$N(p,$\gamma$)$^{14}$O | $^{23}$Na(p,$\alpha$)$^{20}$Ne | $^{22}$Ne($\alpha,\gamma$)$^{26}$Mg | $^{26}$Mg(p,$\gamma$)$^{27}$Al | $^{28}$Si(p,$\gamma$)$^{29}$P |
| $^{17}$O(p,$\alpha$)$^{14}$N | $^{20}$Ne(n,$\gamma$)$^{21}$Ne | $^{22}$Ne($\alpha$,n)$^{25}$Mg | $^{25}$Al(p,$\gamma$)$^{26}$Si | |
| $^{17}$O(p,$\gamma$)$^{18}$F | $^{21}$Ne(p,$\gamma$)$^{22}$Na | $^{23}$Na(p,$\gamma$)$^{24}$Mg | $^{26}$Al(p,$\gamma$)$^{27}$Si | |

Convection was followed using the Ledoux criterion. Semiconvection was modeled as described in (18). Since the treatment of semiconvection is still very uncertain, we computed models using two different assumption for its efficiency: "fast" mixing assumes an efficiency parameter of $\alpha_{\mathrm{sem}} = 0.1$ and overshooting of $0.01 H_P$. This is rather close to the case of convection according to the Schwarzschild criterion. "Slow" mixing (*restricted semiconvection*) assumes an efficiency parameter of only $\alpha_{\mathrm{sem}} = 10^{-4}$. This corresponds, roughly, to a value of 0.04 in the prescription by (10). Unlike (18), we included mass loss by stellar winds into our models according the parameterization of (11).

The nucleosynthesis was followed using a 199 isotope network up to germanium, similar to that used by (18), except that $^{69-70}$Ge were removed and $^{14}$O and $^{19}$Ne were added instead. The nuclear reaction rates were updated for current rates as of 1996 (9, Table 2). In order to obtain the final yield from each star, we followed the evolution and nucleosynthesis form the pre-main sequence until about 1 yr after the supernova explosion.

Since the core collapse itself and the neutron star formation cannot be followed with the KEPLER code, the inner part of the star was removed and replaced by a "piston" when the infall velocity in the core first reached about 1,000 $\mathrm{km\,s^{-1}}$ (18). As described by (18), the location for the piston is chosen such that it coincided with the location of the $Y_e$-discontinuity, typically where $Y_e$ drops below $\sim$0.497. In most cases the $Y_e$-discontinuity coincided with the iron core mass (Table 1).

This "piston" was first moved inward until bounce and then moved outward until it reached a final position of $10^4$ km. The movement of the piston was chosen such that its acceleration is proportional to that of a test particle in the gravitational field of a point mass equal to the mass interior to the piston. For the infall we assumed that the piston reaches its minimum position of 500 km after 0.45 s, and the outward movement was adjusted to give a total explosion energy of $1.2{\cdot}10^{51}$ erg, as observed for SN 1987A (16).

## 3 Nucleosynthesis results and final yields

The production factors of the stable isotopes in our calculation are displayed in Figs. 1 and 2. All unstable isotopes except $^{40}$K were decayed to their stable products. This production factor is defined as the average abundance of all ejecta, including wind, divided by the solar (meteoritic) abundances (5), so that a horizontal line in the figures reproduces solar abundance ratios.

The solar abundances, however, are the result of several generations of stars and supernovae with different metallicities and masses, so that one should not expect a single star to reproduce solar abundance ratios, but only the integral over all masses and metallicities. Nevertheless, models where the production factors lay within a narrow band are preferable and large overproduction of an isotope would be rather problematic. Note also that, as a result of the interaction of the different convective layers and shell sources during the late stellar burning phases, the details of the presupernova structure can sensitively depend on small changes in the initial properties of the star and may cause discontinuous changes in the core sizes (Table 1) and the resulting yields. Against this background, the models presented here have to be considered as stochastically picked, hopefully typical, but not necessarily average, cases around the given initial masses, metallicity and rotational properties, and taking into account our other model assumptions.

Both 15 $\mathrm{M_\odot}$ models with restricted semiconvection (db15 and eb15) show a

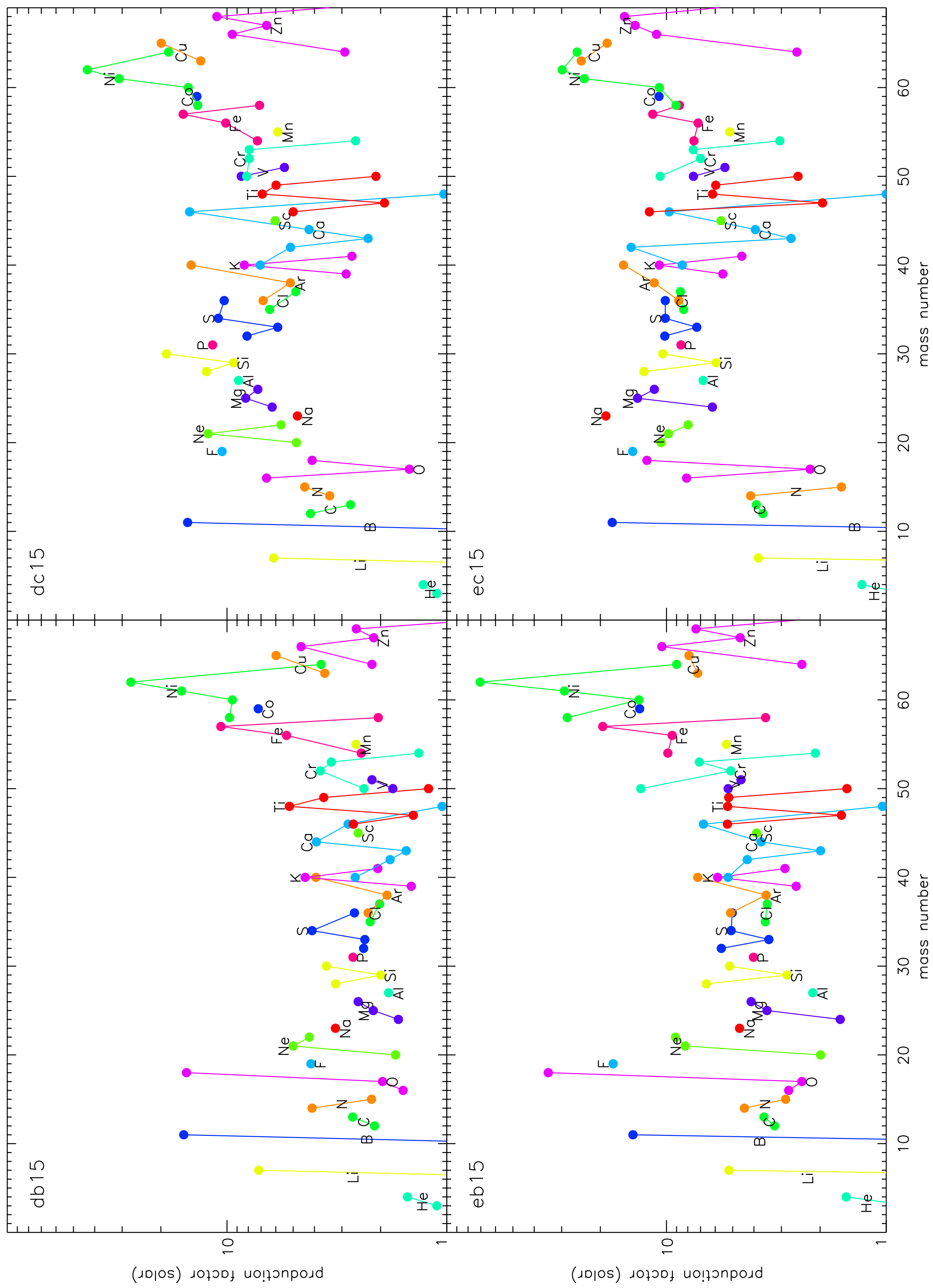


Fig. 1. Production factors (abundance of all ejecta, including wind, relative to solar abundance) for our $15\,\mathrm{M}_\odot$ models. In this matrix the e?15 models are rotating stars while the d?15 models are non-rotating. The second character ("?") indicates slow ("b") or fast ("c") semiconvection. See also Table 1.

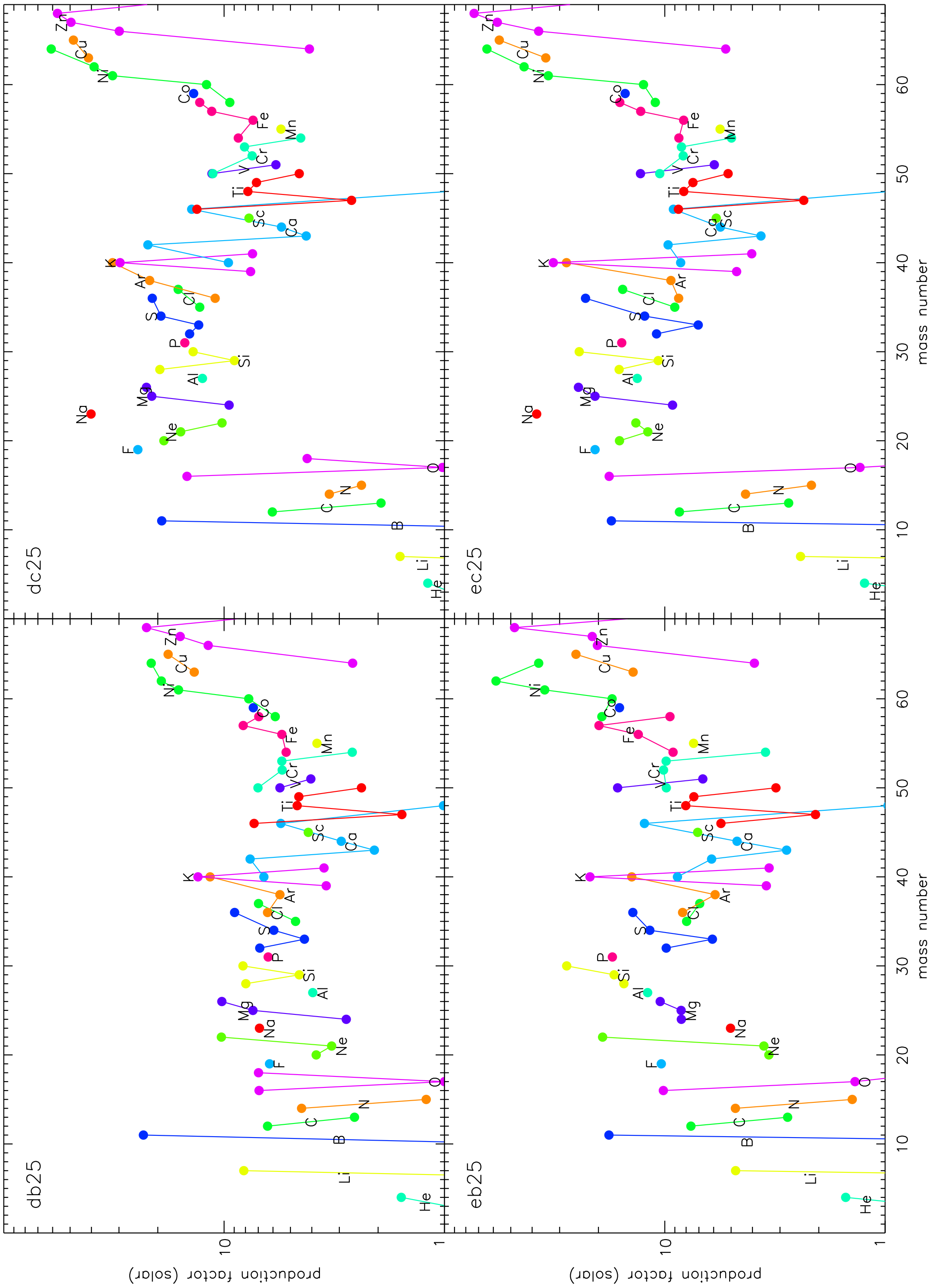


Fig. 2. Production factors (abundance of all ejecta, including wind, relative to solar abundance) for our $25\,M_{\odot}$ models. See also Table 1.

problematic overproduction of $^{18}$O and $^{62}$Ni. The "fast" semiconvection models (Models dc15 and ec25) clearly give better results. The differences between the rotating and non-rotating models are much smaller. Model dc25 shows high yields of Ni, $^{21}$Ne, $^{30}$Si, $^{40}$Ar, and $^{46}$Ca, while in Model ec25 only the sodium is somewhat overabundant.

For the 25 $M_\odot$ stars the non-rotating model with "slow" semiconvection (db25) gives the most solar-like relative abundance distribution. However, this models model also showed the most fallback (0.25 $M_\odot$), while in the rotating models no fallback occurred. Model S25A from (18), which is similar to Model dc25 except for the missing mass loss, had 0.29 $M_\odot$ of fallback (Table 1) onto a 0.1 $M_\odot$ bigger iron core compared to Model dc25, where only $\sim$0.06 $M_\odot$ fell back. This is reflects in the amount of iron group elements ejected by the star. The two rotating models produce about twice as much of the heavy Ni isotopes and of Cu and Zn than in Model db25. The dip in the production factor at Ca...Co realtive to the lighter isotopes seems not to be correlated to the amount of fallback in our models, but more expressed in the rotating stars. The rotation also affects the production of the elements in the range Ne to Ar. Both rotating Models show a strong overabundance of $^{23}$Na, and all the 25 $M_\odot$ stars were efficient producers of $^{40}$K.

A feature common to all our models is the apparent overproduction of the isotopes just above the iron group, similar to what has been found by (18). The reason for this is not yet understood. Especially in the 25 $M_\odot$ star models the elements towards the end of the network (Zn) are strongly over-abundant. This has to be investigated in more detail in future calculations using larger networks.

## 4 Conclusions

Rotation and mass loss both affect the nucleosynthetic yields of massive stars. For the case of a 15 $M_\odot$ star "fast" semiconvection and rotation gave the best result in the sense that the abundance ratio in the ejected mass reproduces solar abundance ratios. For the 25 $M_\odot$ stars the picture is much less clear. In this case, the same model parameters lead to a large overproduction of the heavy iron group isotopes, due to the absence of any fallback in this model. These isotopes are, however, located at the end of our network. Except for the overproduction of $^{23}$Na (and, to some lower extend, also $^{40}$Ar and $^{40}$K) this model still reproduces solar abundance ratios within a factor of $\sim$2. A more extended discussion of these models will be presented in (8).

For given assumptions of the input physics, the presupernova structure of the stars can change discontinuously as a function of its initial parameters, and therefore each model stands for a typical case around its mass, but not an average. To reproduce galactochemical evolution – and the solar abundance pattern – one has to integrate over a fine grid of initial masses with different rotation velocities and metallicities.

A further uncertainty comes from our assumption that all models produce the same final kinetic energy of the ejecta, $1.2 \cdot 10^{51}$ erg, but the different presupernova structures might well result in variations of the explosion energies as well (2), which, in turn, changes the nucleosynthesis and the amount of fall-back. On the other hand, also rotation in the core affects the dynamics of the explosion and can lead to asymmetric supernova explosions (3). Both effects where not taken into account here.

Our rotating stellar models kept a considerable amount of angular momentum in the core up to the supernova stage, in most cases more angular momentum than a critically rotating neutron star could have (7). In case a black hole forms during the core collapse, we found sufficient angular momentum to form an accretion disk around this black hole which may lead to the formation of a jet either by neutrino-annihilation of by magnetic fields (12). This may lead to an asymmetric, jet-driven supernova (19), or, in case the star has lost its hydrogen-rich envelope, even a gamma-ray burst can result (12, for details).

**Acknowledgments.** This research was supported, in part, by Prime Contract No. W-7405-ENG-48 between The Regents of the University of California and the United States Department of Energy, by the grants from the National Science Foundation (AST 97-31569 and INT-97-26315), and by the Alexander von Humboldt-Stiftung (FLF-1065004).

## References

[1] Endal, A. S., Sofia, S. (1978), *ApJ* **220** 279.
[2] Fryer, C. L. (1999) *ApJ* **522** 413.
[3] Fryer, C. L., Heger, A. (1999) *ApJ*, submitted.
[4] Fukuda, I. (1982), *PASP* **94** 271.
[5] Grevesse, N., Noels, A. (1993) in *Origin and Evolution of the Elements*, ed. N. Prantzo, E. Vangioni-Flam, M. Casse (Cambridge: Cambridge Univ. Press), p. 13.
[6] Heger, A. (1998) *PhD thesis* Technische Universität München.
[7] Heger, A., Langer, N., Woosley, S. E. (2000) *ApJ* **528** in press.
[8] Heger, A., Woosley, S. E., Langer, N. (2000) *ApJ* in preparation.
[9] Hoffman, R. D., Woosley, S. E. (2000) *ApJ*, in preparation.
[10] Langer, N., Sugimoto, D., Fricke, K. J. (1983), *A&A* **126** 207
[11] Nieuwenhuijzen, H., de Jager, C. (1990), *A&A* **231** 134.

[12] MacFadyen, A. I., Woosley, S. E. (1999) A. *ApJ* **524** 262.
[13] Pinsonneault, M. H., Kawaler, S. D., Sofia, S., Demarque, P. (1989), *ApJ* **338** 424.
[14] Weaver, T. A., Woosley, S. E. (1993) *Phys. Rep.* **227** 65.
[15] Weaver, T. A., Zimmerman, G. B., Woosley, S. E. (1978) *ApJ* **225** 1021.
[16] Woosley, S. E. (1988) *ApJ* **330** 218.
[17] Woosley, S. E., Weaver, T. A. (1988) *Phys. Rep.* **163** 79.
[18] Woosley, S. E., Weaver, T. A. (1995) *ApJS* **101** 181.
[19] Woosley, S. E., MacFadyen, A. I., Heger, A. (2000) *ApJ*, submitted.